Effect of the Dirac-cone tilt on the disorder-broadened Landau levels in a two-dimensional Dirac nodal system

Haibo Yao, Mingfeng Zhu, Liwei Jiang, and Yisong Zheng*
Key Laboratory of Physics and Technology for Advanced Batteries (Ministry of Education), Department of Physics, Jilin University, Changchun 130012, China

(Received 12 July 2021; accepted 29 November 2021; published 7 December 2021)

By means of the kernel polynomial method (KPM), a numerically exact theoretical approach, we calculate the density of states (DOS) and diagonal conductivity of a two-dimensional Dirac nodal system in the presence of a high magnetic field. The effect of Dirac cone tilt on the profiles of disorder-broadened Landau level (LL) peaks in both the DOS and diagonal conductivity spectra is our main concern. Our numerical results show that the profile of an isolated LL peak in DOS, especially the $n = 0$ one, is tilt independent. On the other hand, the Dirac cone tilt enhances/reduces the diagonal conductivity peaks in the direction perpendicular/parallel to the cone tilt direction (y direction). In particular, at the Dirac point, i.e., zero energy, the ratio of the former to the latter is $\sigma_{xx}(0)/\sigma_{yy}(0) = 1/(1-\beta^2)$, with β being the tilt parameter. In addition, in comparison with the results obtained by KPM, we check the validity of the self-consistent Born approximation (SCBA) which has thus far been widely exploited for studying the DOS and quantum transport properties of Dirac or Weyl systems with disorder. We find that the SCBA fails to describe the detail of the LL peak around zero energy. At zero energy, the KPM result of the diagonal conductivity increases with the disorder strength before saturation, rather than a disorder-independent constant as reported previously by SCBA.

DOI: 10.1103/PhysRevB.104.235406

I. INTRODUCTION

In recent years, two-dimensional (2D) topological semimetal materials have attracted intense research interest due to their peculiar band structures and potential applications in nanoelectronics. As a paragon of 2D topological semimetals, graphene's conduction and valence bands exhibit an almost perfect cone shape near the Dirac point [1,2], which is called a Dirac cone. The massless Dirac fermion nature remarkably manifests itself in the high magnetic field, where the Dirac cone is quantized into a set of nonequidistant Landau levels (LLs) given by $E_n = \mathrm{sgn}(n)\sqrt{2e\hbar v_F^2|n|B}$, where e is electron charge, $\hbar$ is the Planck's constant, v_F is the Fermi velocity, $n = 0, \pm1, \pm2\cdots$ is the LL index, and B is the magnetic field strength. This emblematic LL spectrum and its characteristic zero energy ($n = 0$) LL are directly related to the half-integer quantum Hall effect in graphene [3]. Many efforts have been made to determine the electronic properties of the disorder-broadened LLs. In previous works [4,5], Zhu *et al.* exactly calculated the density of states (DOS) of graphene under a high magnetic field and white-noise random potential using the Lanczos recursive method. The results show that the zero-energy LL peak in the DOS spectrum has a Gaussian shape, which is similar to the Gaussian-like shape for the lowest LL for the conventional 2D Schrodinger electrons [6], and the broadening width Γ of the LL peak depends on both the magnetic field and the disorder. Specifically, Γ is proportional to the random potential variance and the square root of the magnetic field strength [4,5]. According to such characteristics of the zero-energy LL peak in DOS, it is deduced that the diagonal conductivity at zero energy (Dirac point) in graphene does not depend on the magnetic field strength and is only disorder dependent in high magnetic field environments [4]. Later, Ortmann and Roche further proved that the zero-energy diagonal conductivity in disordered graphene is saturated in high magnetic field when disorder strength increases to a certain extent through rigorous numerical simulation for Kubo conductivity [7].

In fact, in many realistic Dirac materials, the Dirac cone is more or less distorted. It is known that tilted Dirac cones appear in a number of materials, including graphene under uniaxial strain [8], partially hydrogenated graphene [9], layered organic conductor α-$(BEDT\text{-}TTF)_2I_3$ [10–13], 8-$Pmmn$ borophene [14–17], and the surface of topological crystalline insulators [18,19]. Recent studies have revealed that the tilt of the Dirac cone brings some observable effects, such as unconventional Klein tunneling [20,21], anisotropic Friedel oscillations [22], anisotropic optical conductivity [23], and enhanced frequency of Weiss oscillation [17]. So far, how the Dirac cone tilt affects the disorder-broadened LL peaks in both the DOS and diagonal conductivity spectra of a disordered 2D Dirac nodal system has not been explored, which is the focus of this paper.

In this paper, using the kernel polynomial method (KPM), a numerically exact theoretical approach, we calculate the DOS and diagonal conductivity of a 2D Dirac system model that hosts two Dirac cones with adjustable tilt under high magnetic field and random on-site disorder. Our numerical results on DOS show that the tilt of the Dirac cone squeezes the LL spectrum and densifies the LL peaks, which drives the system to leave the quantum Hall regime under relatively weak

*Corresponding author: zhengys@jlu.edu.cn

disorder. However, in the quantum Hall regime, the broadening of the isolated zero-energy LL peak is tilt independent. As a result, its features are similar to that of graphene. To study the relationship between the diagonal conductivity and Dirac cone tilt, the diagonal conductivities parallel and perpendicular to the cone tilt direction are calculated numerically. As expected, the diagonal conductivity exhibits tilt-dependent anisotropy. The tilt of the Dirac cone enhances the diagonal conductivity in the direction perpendicular to the cone tilt but reduces the diagonal conductivity parallel to the cone tilt direction. At zero energy, the ratio of the former to the latter is $1/(1-\beta^2)$, with β being the tilt parameter. By comparison, the anisotropy of the diagonal conductivity in the energy range of nonzero LLs is relatively weak. In addition, based on the results obtained by using KPM, we test the validity of the self-consistent Born approximation (SCBA), which has thus far been widely exploited for studying the DOS and quantum transport properties of Dirac or Weyl systems with disorder [24–31] and has been found to fail to give accurate results for physics near the Dirac point in the absence of magnetic field [32]. We find that the SCBA fails to describe the details of the LL peak around zero energy in the presence of magnetic field.

This paper is organized as follows. In Sec. II, the continuous and lattice Hamiltonian of a 2D Dirac system model with two tilted Dirac cones are specified and a theoretical analysis of the anisotropy of diagonal conductivity in the clean system is given. In Sec. III, we show and discuss the numerical results of the DOS and diagonal conductivity spectra, where the results within SCBA are also presented in comparison with those from KPM. Finally, we summarize our main outcomes in Sec. IV. To understand the anisotropy of the diagonal conductivity, the eigensolutions of the effective Hamiltonian in the presence of a magnetic field and the matrix elements of the velocity operator in the eigenrepresentation are presented in Appendix A. The KPM to determine the DOS and diagonal conductivity is elaborated in Appendix B, while the expressions of these two quantities within SCBA are given in Appendix C.

II. MODEL AND METHODS

We start from the model Hamiltonian that hosts two Dirac cones. The model Hamiltonian is constructed on a 2D square lattice with two orbitals on each site. Taking the lattice constant a_0 as unit length, the Hamiltonian reads

$$\begin{aligned} H_0(\boldsymbol{k}) =& 2t(\cos k_x\sigma_x + \sin k_y\sigma_y) \\ &+ m_0(1-\cos k_y)\sigma_x + 2t_y \sin k_y\sigma_0, \end{aligned} \tag{1}$$

where t is the hopping parameter between the nearest-neighbor sites, the Pauli matrices σ_x, σ_y and identity matrix σ_0 act on the orbital space, the mass term m_0 is introduced to open a finite energy window so as to avoid the band overlapping, and the last term with t_y denotes the tilt of the spectrum. The two Dirac cones are located at $K_\eta = (\eta\pi/2, 0)$ with $\eta = \pm$. In the absence of the tilt term, this model preserves the inversion symmetry $H_0(\boldsymbol{k}) = \sigma_x H_0(-\boldsymbol{k})\sigma_x$. The introduction of the tilt term makes the two Dirac cones anisotropic and breaks the inversion symmetry. The Dirac cones are set to tilt in the k_y direction, perpendicular to the line connecting the two Dirac nodes. Such a tilt ensures that the two Dirac cones do not overlap each other until they are tipped over. Around the Dirac node K_η, $H_0(\boldsymbol{k})$ can be expanded to yield an effective low-energy description,

$$H_{0\eta}(\widetilde{\boldsymbol{k}}) = \gamma(-\eta\widetilde{k}_x\sigma_x + \widetilde{k}_y\sigma_y + \beta\widetilde{k}_y\sigma_0), \tag{2}$$

with $\gamma = 2t$, $\beta = t_y/t$ being the tilt parameter and $(\widetilde{k}_x, \widetilde{k}_y)$ being the effective wave vector with the origin at the Dirac node K_η. According to literature [13,17], the effective tilt parameters in 8-*Pmmn* borophene and a-$(BEDT\text{-}TTF)_2I_3$ materials can reach 0.41 and 0.76, respectively.

In the presence of a magnetic field, it is difficult to solve the eigenequation of the $H_{0\eta}(\widetilde{\boldsymbol{k}})$ with an introduced magnetic vector potential due to the existence of the tilt term. Fortunately, there is a Lorentz boost method which can solve this problem strictly [33]. By means of this method, we obtain the eigensolutions and show them in Appendix A. The LLs are $\varepsilon_n = \mathrm{sgn}(n)\sqrt{2|n|}\gamma(1-\beta^2)^{3/4}l_B^{-1}$ with $n = 0, \pm1, \pm2...$ being Landau index and $l_B = \sqrt{\hbar/eB}$ being the magnetic length. Compared with the LLs of graphene, this result reveals that the tilt of the Dirac cone has an effect of squeezing the LL spectrum, as one can see from the factor $(1-\beta^2)^{3/4} < 1$. As β evolves from 0 to 1, the LL spectrum becomes gradually denser. When $\beta \to 1$, i.e., the Dirac cone is tipped over, the whole quantized LL spectrum collapses, regardless of the magnetic field strength. As a note, the LL solution above is valid only for $\beta \leqslant 1$. For $\beta > 1$, i.e., the dispersion becomes type II, the Hamiltonian given in Eq. (2) has no quantized eigenenergies in the presence of magnetic field, because its energy dispersion in the zero field gives an open Fermi surface, on which the closed semiclassical cyclotron orbit cannot be formed. If we adopt an improved model for a Hamiltonian with a closed Fermi surface, such as Eq. (1), it can be seen that the quantized LLs still exist even in the case of $\beta > 1$, although they may be very dense. Just like the LLs with $k_z = 0$ of the 3D Weyl system reported in Refs. [34,35], they are characterized by the eight-shaped semiclassical cyclotron orbit jointly provided by the electron pocket and hole pocket. Considering the fact that the type-II Dirac cone has not been observed in 2D materials, we mainly discuss the case of $\beta < 1$ in this paper.

To simulate the disordered sample, we express the Hamiltonian in the lattice space. On a 2D square lattice with finite size $N_x \times N_y$ and the periodic boundary condition, $H_0(\boldsymbol{k})$, as given by Eq. (1), is discretized as

$$\begin{aligned} H_0 = \sum_{\boldsymbol{r},s,s'} \Big\{ \Big[& C^\dagger_{\boldsymbol{r}+\hat{x},s} t\sigma^x_{ss'} C_{\boldsymbol{r},s'} \\ & + C^\dagger_{\boldsymbol{r}+\hat{y},s}\Big(-it\sigma^y_{ss'} - \frac{m_0}{2}\sigma^x_{ss'} - it_y\sigma^0_{ss'}\Big) C_{\boldsymbol{r},s'}\Big] \\ & + h.c. + C^\dagger_{\boldsymbol{r},s} m_0\sigma^x_{ss'} C_{\boldsymbol{r},s'} \Big\}, \end{aligned} \tag{3}$$

where $\boldsymbol{r} = (x, y)$ is the coordinate on the square lattice, $\hat{x}$ and $\hat{y}$ are the lattice vectors along the x and y directions, respectively. The magnetic field is incorporated by means of Peierls substitution in the hopping parameter as $t \to te^{i\phi(\boldsymbol{r})}$, where $\phi(\boldsymbol{r}) = e/\hbar \int_{\boldsymbol{r}}^{\boldsymbol{r}+\hat{x}/\hat{y}} \boldsymbol{A}\cdot d\boldsymbol{r}'$. Under the Landau gauge of the vector potential $\boldsymbol{A} = (-yB, 0, 0)$, only the hopping

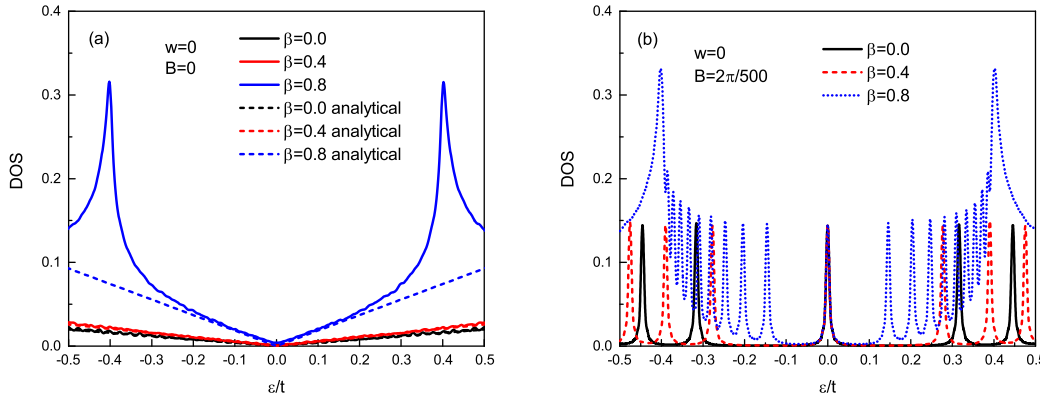

FIG. 1. The DOS spectra of the 2D Dirac system with typical cone tilt given by Eq. (1) in the absence of the magnetic field (a) and in the presence of the magnetic field (b). In (a), the analytical results derived from the effective Hamiltonian given by Eq. (2) are also shown for comparison, which is $\rho(\varepsilon) = \varepsilon/8\pi t^2(1-\beta^2)^{3/2}$.

parameter t along the x direction is replaced by $te^{-ieyBa_0/\hbar}$. To be commensurate with the lattice structure, the magnetic field is commonly written as $B = 2\pi/N_y$, with the unit of $\hbar/ea_0^2$. We consider the random on-site disorder potential as

$$H_d = \sum_{\boldsymbol{r},s} \varepsilon_{\boldsymbol{r},s} C^\dagger_{\boldsymbol{r},s} C_{\boldsymbol{r},s}, \tag{4}$$

where $\varepsilon_{\boldsymbol{r},s}$ is randomly distributed in the range of $[-w/2, w/2]$, w gives the disorder strength. Such a disorder is widely adopted in Dirac and Weyl systems [4,31,36,37].

Based on the lattice Hamiltonian, we prepare to numerically simulate the system's DOS and diagonal conductivity $\sigma_{\alpha\alpha}$ with $\alpha = x, y$ using the Kubo-Greenwood formula. The DOS is given by

$$\rho(\varepsilon) = \frac{1}{N}\langle \mathrm{Tr}[\delta(\varepsilon - H)]\rangle, \tag{5}$$

where $\langle\rangle$ means the average of disordered samples, $H = H_0 + H_d$, and $N = 2N_xN_y$ is the dimension of the system. The diagonal conductivity is written in the form

$$\sigma_{\alpha\alpha}(\varepsilon) = \frac{\pi\hbar e^2}{S}\langle \mathrm{Tr}[v_\alpha \delta(\varepsilon - H) v_\alpha \delta(\varepsilon - H)]\rangle, \tag{6}$$

where S is the area of the system and $v_\alpha = [\alpha, H]/i\hbar$ denotes the α component of the velocity operator. In Appendix B, we elaborate on the numerical recipe to obtain these two quantities within KPM [38,39], while their expressions within SCBA are given in Appendix C.

Before performing the numerical simulation, it makes sense for us to analyze the anisotropy of diagonal conductivity caused by the tilt of the Dirac cone in a clean system. To do this, we start with the effective Hamiltonian given by Eq. (2), whose eigenfunctions in the presence of a magnetic field are shown in Eqs. (A4)–(A7) in Appendix A. Using these eigenfunctions as a basis set, the diagonal conductivity is expressed as

$$\sigma_{\alpha\alpha}(\varepsilon) = \frac{\pi\hbar e^2}{S}\sum_{n,n',k_y} \langle nk_y|v_\alpha|n'k_y\rangle \times \delta(\varepsilon - \varepsilon_{n'})\langle n'k_y|v_\alpha|nk_y\rangle\delta(\varepsilon - \varepsilon_n), \tag{7}$$

where $n(n')$ denotes the Landau index, k_y denotes the momentum along y direction which is conserved under the Landau gauge, and $\delta(\varepsilon - \varepsilon_n) = \eta/\pi[(\varepsilon - \varepsilon_n)^2 + \eta^2]$ with $\eta \to 0^+$. When the Fermi energy is at the nth LL,

$$\sigma_{\alpha\alpha}(\varepsilon_n) = \frac{\hbar e^2}{\pi S}\sum_{n'\neq n,k_y} \frac{|\langle nk_y|v_\alpha|n'k_y\rangle|^2}{[(\varepsilon_n - \varepsilon_{n'})^2 + \eta^2]}, \tag{8}$$

where the $n' = n$ term is removed from the summation because the expectation value of the velocity operator at a LL is always zero. The matrix elements of the velocity operator $\langle nk_y|v_\alpha|n'k_y\rangle$ with $\alpha = x$ and y are given in Eqs. (A8) and (A9) in Appendix A, respectively. It is not difficult to find that both $\sigma_{xx}(\varepsilon_n)$ and $\sigma_{yy}(\varepsilon_n)$ are β dependent and $\sigma_{xx}(\varepsilon_n) \neq \sigma_{yy}(\varepsilon_n)$. As can be seen from Eqs. (A8) and (A9), $|\langle 0k_y|v_x|n'k_y\rangle|^2/|\langle 0k_y|v_y|n'k_y\rangle|^2 = 1/(1-\beta^2)$ always holds for $n' \neq 0$. As a result, one has $\sigma_{xx}(0)/\sigma_{yy}(0) = 1/(1-\beta^2)$. In contrast, if $n \neq 0$ and $\mathrm{sgn}(nn') > 0$, we can readily find the following constraint: $|\langle nk_y|v_x|n'k_y\rangle|^2/|\langle nk_y|v_y|n'k_y\rangle|^2 < 1/(1-\beta^2)$. According to the denominator $(\varepsilon_n - \varepsilon_{n'})^2 + \eta^2$ in Eq. (8) and the velocity matrix element formula Eqs. (A8) and (A9), the diagonal conductivity at a LL is mainly contributed by the nearest LL. Consequently, we get $\sigma_{xx}(\varepsilon_n)/\sigma_{yy}(\varepsilon_n) < 1/(1-\beta^2)$ for $n \neq 0$.

III. RESULTS AND DISCUSSIONS

A. DOS

First, let us show the numerical result of the DOS spectrum of the 2D Dirac system model without disorder. Figure 1(a) shows the DOS spectra of three systems with tilt parameters $\beta = 0$, 0.4, and 0.8 in the absence of magnetic field. Here, the analytical results derived from the effective Hamiltonian given by Eq. (2) are also shown for comparison, which is $\rho(\varepsilon) = \varepsilon/8\pi t^2(1-\beta^2)^{3/2}$. It can be seen that the numerical results from KPM still have a slight Gibbs oscillation after introducing the Lorentz kernel. When β increases from 0 to 0.8, the DOS near zero energy increases gradually, which can be attributed to the increase of the area of the isoenergetic cross section caused by the tilt of the Dirac cone. Meanwhile, the energy range of the linear dispersion of the model is reduced. Especially for $\beta = 0.8$, the linear dispersion is only

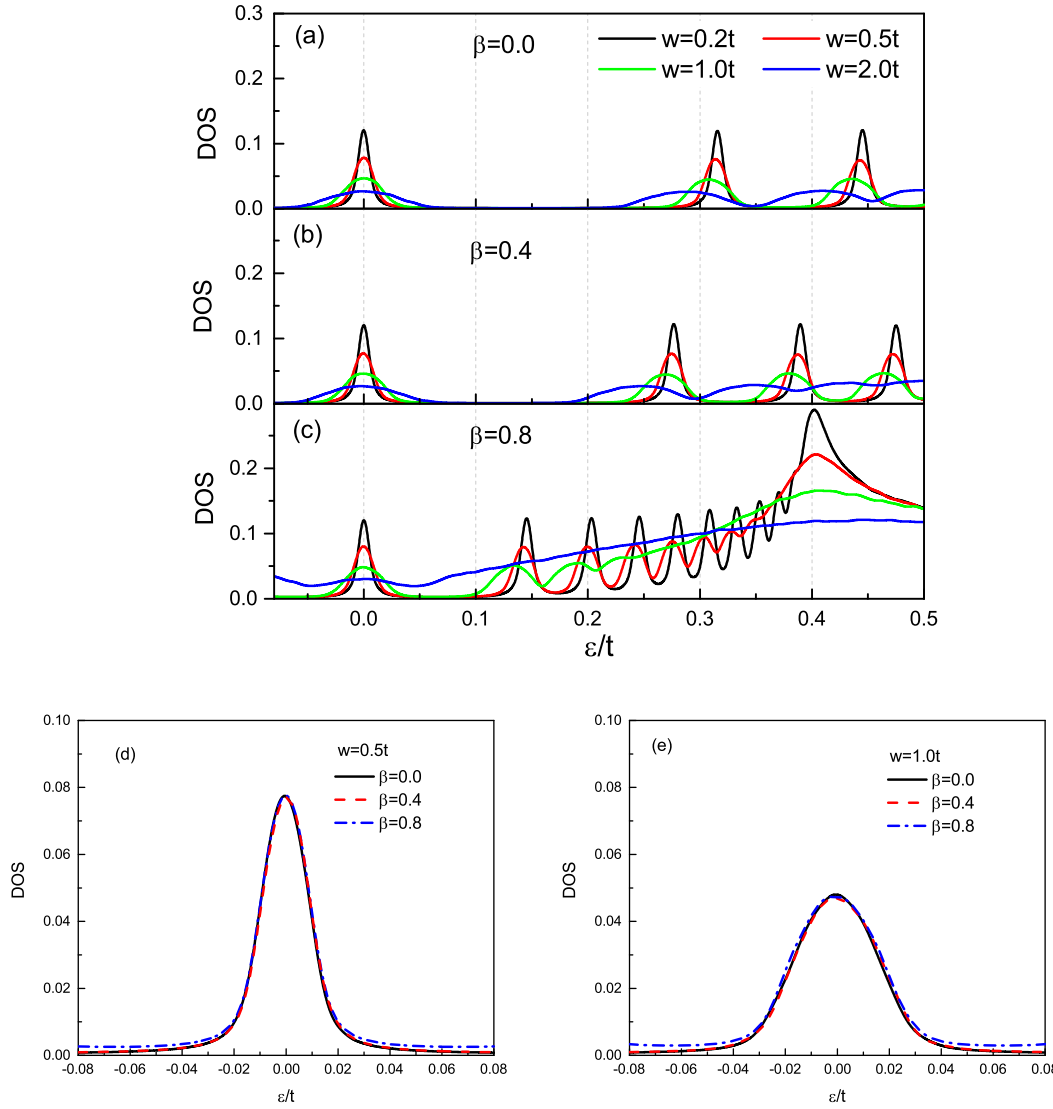

FIG. 2. (a)–(c) The evolution of the LL peaks with the disorder strength w at $B = 2\pi/500$. (a)–(c) correspond to the systems with $\beta = 0$, 0.4, and 0.8, respectively. (d), (e) A comparison of the zero-energy LL peaks of three systems in the cases of $w = 0.5t$ and $1.0t$, respectively.

maintained in the $(-0.2t, 0.2t)$ energy range. When a strong magnetic field is present, the DOS of these three systems exhibit the quantized LL spectra, as shown in Fig. 1(b). Here, the nonzero width of each LL is due to the truncation of the Chebyshev polynomial mentioned above. As expected, the larger the tilt, that is, the larger β, the denser the LLs. However, for the system with $\beta = 0.8$, the LL peaks away from zero energy are significantly overlapped with each other because they are too dense. Especially, in the vicinity of the van Hove singularity $\varepsilon = \pm 0.4t$, the LL peaks are indistinguishable due to the excessive overlap, resulting in a similar DOS profile as that in the case without magnetic field.

Now we focus on the feature of the disorder-broadened LL peak in the DOS spectrum. Figure 2 shows the evolution of the LL peak with the disorder strength w at $B = 2\pi/500$, where Figs. 2(a)–2(c) correspond to the systems with $\beta = 0$, 0.4, and 0.8, respectively. As can be seen from Fig. 2(a), each LL peak is gradually broadened as w increases from $0.2t$ to $2.0t$. Meanwhile, the peak height is reduced because the total number of states in each LL remains constant. When w increases to $2.0t$, the LL peak of $n = 1$ starts to overlap with the next LL peak, and only the LL peak of $n = 0$ is isolated. In addition to the broadening in width, all the LL peaks except the $n = 0$ one move toward zero energy, which is called the redshift of the LL peak and was also observed in graphene [4]. The redshift increases with w. Results presented in Fig. 2(b) are similar to those in Fig. 2(a), except that the LL peaks are denser. In contrast, in Fig. 2(c), in the cases of small w, such as $w \leqslant 1.0t$, the LL peaks away from zero energy overlap with the nearest LL peaks significantly, resulting in very different LL peak profiles. Because the LL peak of $n = 0$ is relatively far away from its nearest LL peaks, it remains isolated. When w increases to $2.0t$, the DOS shows a continuous energy spectrum, which means that the tilt of the Dirac cone drives the system away from the quantum Hall regime. Notice that in the quantum Hall regime, the isolated zero energy LL peak in Fig. 2(c) is the same as those in Figs. 2(a) and 2(b) for a given w. As a verification, in Figs. 2(d) and 2(e), we compare the zero-energy LL peaks of these three systems in the cases of $w = 0.5t$ and $1.0t$, respectively. As shown in these two

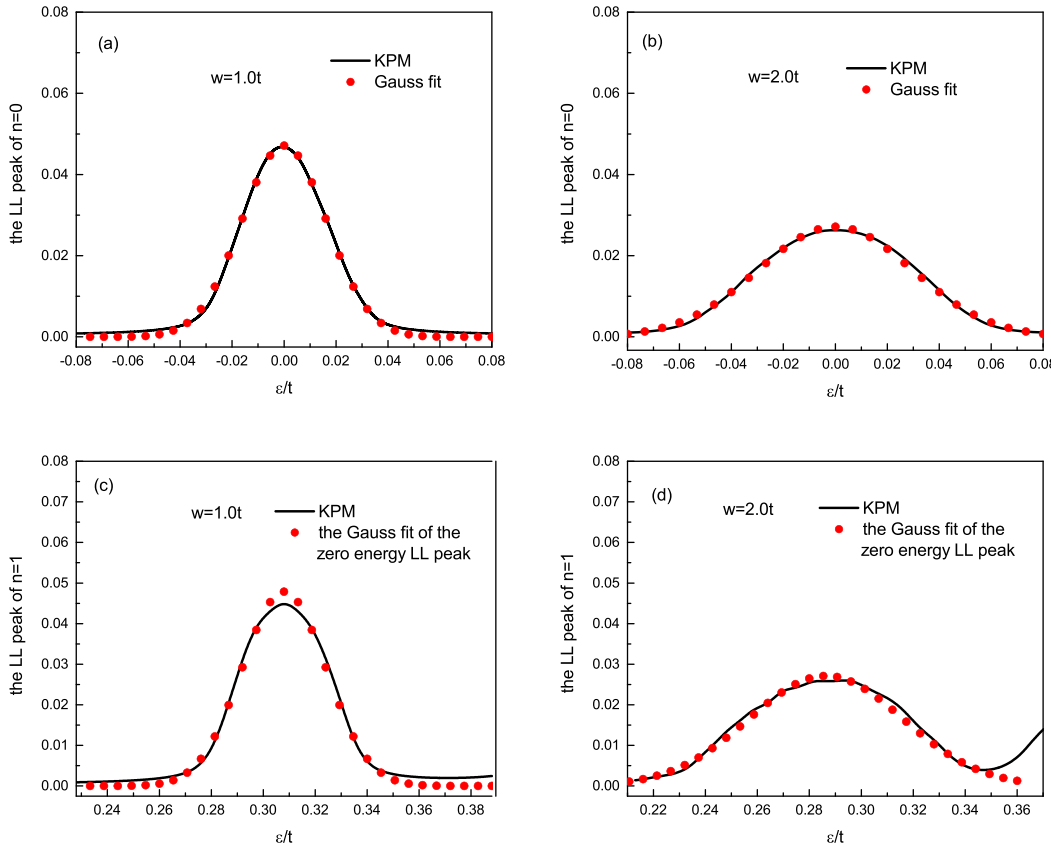

FIG. 3. (a), (b) The zero-energy LL peak in the system with $\beta = 0$ in the cases of $w = 1.0t$ and $2.0t$, respectively. In both cases, the profile of the LL peak is well fitted by the Gaussian function $C\exp(-\varepsilon^2/2\Gamma^2)/\Gamma$ with C and Γ being fitting parameters. (c), (d) The LL peak of $n = 1$ in the cases of $w = 1.0t$ and $2.0t$, respectively. Here, the red dots is the Gaussian fitting of the zero-energy LL peak which is shifted to the position of LL peak of $n = 1$.

figures, the three curves are nearly identical except that the result of $\beta = 0.8$ shows a slightly cocked tail at the end of the LL peak due to the overlap of the next LL peak. To sum up, we can say that the profile of the isolated LL peak in the DOS spectrum does not depend on the tilt of the Dirac cone.

Next, we pay attention to the shape of the isolated LL peak in the DOS spectrum. Since the profile of the zero-energy LL peak is tilt independent, we choose the system with $\beta = 0$ to check the shape of the LL peak. Figures 3(a) and 3(b) show the zero-energy LL peak in the cases of $w = 1.0t$ and $2.0t$, respectively. As shown by the red dots, the profile of the LL peak can be well fitted by a Gaussian function in both cases. Such a shape of the zero-energy LL peak is consistent with that of graphene calculated by the Lanczos recursive method [4]. Furthermore, we show the LL peak of $n = 1$ in these two cases in Figs. 3(c) and 3(d) to check whether they follow the same feature as the zero-energy LL peak. We can see that the profile of the LL peak of $n = 1$ is slightly deviated from the Gaussian fitting curve of the zero-energy LL peak in both cases, which indicates that the profile of the nonzero LL peak is not exactly the same as that of the zero-energy LL peak due to the influence of the next LL peak. Therefore, it can be predicted that the tilt of the Dirac cone will aggravate the deviation between shapes of the nonzero LL peak and the zero-energy LL peak because of the stronger influence of the nearest LL peak.

We now test the validity of SCBA in determining the DOS of a 2D Dirac system under magnetic field and disorder. To compare with the results from KPM, we set the infinitesimal η in Green's function to be $\eta = 4 \times 10^{-3}t$ in SCBA, which gives the same artificial width of LL peak in clean system as in KPM. In Fig. 4(a), we compare the DOS of the system with $\beta = 0$ computed by the two methods for various w. We can see that for all the considered w's, in which cases the system is in the quantum Hall regime, the two sets of data are in agreement in terms of the broadenings and the redshifts of the LL peaks. Even in the $w = 4.0t$ case, in which the system leaves the quantum Hall regime, the DOS from SCBA deviates slightly from the result from KPM which occur in the energy regions near $\pm 0.1t$ and far away from zero energy. If we take care of the details of each LL peak, the two kinds of result show differences to some extent. To show this clearly, we compare the zero-energy LL peaks from the two methods in the cases of $w = 1.0t$ and $2.0t$ in Fig. 4(b). The zero-energy LL peak from SCBA is close to a semielliptical type rather than Gaussian type as in KPM. The semielliptical shape of LL peak is a well-known conclusion within SCBA [24]. Due to the difference in shape, the DOS at zero energy from SCBA is always smaller than that from KPM. However, the difference between the two kinds of results degrades at higher energies, as seen in Fig. 4(a). Therefore, SCBA is not competent to describe the shape of the zero-energy LL peak in detail. For

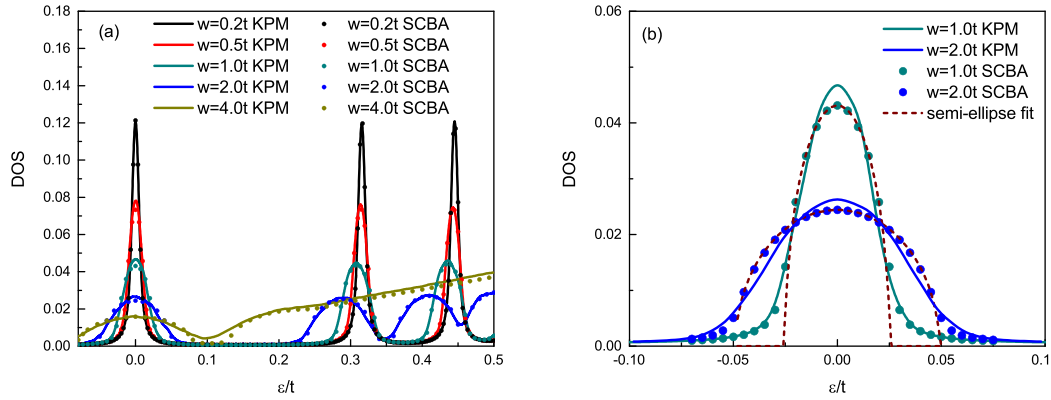

FIG. 4. (a) A comparison of the DOS computed by KPM and SCBA with $\beta = 0$ and $B = 2\pi/500$. (b) Enlarged views of the LL peaks of $n = 0$ for the cases of $w = 0.1t$ and $2.0t$ in (a). Here, the numerical results from SCBA are fitted by a semielliptical function $C\sqrt{1-\varepsilon^2/\Gamma^2}/\Gamma$.

nonzero LL peaks, their profiles are not exactly the same as those of the zero-energy LL peak due to the influence of the nearest LL peaks, but the results from the two methods are consistent.

In Fig. 5(a), we compare the DOS spectra of the three systems with $\beta = 0$, 0.4, and 0.8 at $w = 1.0t$ computed by the two methods. It can be seen that even for the system with tilt, the DOS spectra from the two methods are still in agreement. To see clearly the details near zero energy, we show enlarged views of the zero-energy LL peaks in Fig. 5(b). Because the KPM result of the LL peak is β-independent, only the KPM result of the system with $\beta = 0$ is shown here. It can be seen that under SCBA, the LL peak of the system with $\beta = 0$ and 0.4 is nearly identical, but the LL peak of the system with $\beta = 0.8$ is slightly higher than them. By comparison, at zero energy, the SCBA result of the system with $\beta = 0.8$ is closer to the KPM result.

B. Diagonal conductivity

As discussed in Sec. II, the tilt of the Dirac cone results in a tilt-dependent and anisotropic diagonal conductivity in a clean system. Accordingly, one may wonder to know the anisotropy of the diagonal conductivity in a disordered system. With such a purpose, we calculate σ_{xx} and σ_{yy} of the disordered systems with various tilts. Figures 6(a) and 6(b) show the calculated σ_{xx} and σ_{yy} as functions of Fermi energy ε for the three systems with $\beta = 0$, 0.4, and 0.8, respectively. Here, the disorder strength and magnetic field are fixed at $w = 1.0t$ and $B = 2\pi/500$, respectively. As can be seen in Fig. 6(a), $\sigma_{xx}(\varepsilon)$ of each system presents a set of disorder-broadened LL peaks. Compared with $\sigma_{xx}(\varepsilon)$ of the systems with $\beta = 0$ and 0.4, $\sigma_{xx}(\varepsilon)$ of the system with $\beta = 0.8$ shows that the nonzero LL peak overlaps with the adjacent LL peaks remarkably, which is consistent with the behavior of the LL peaks in the DOS spectrum in Fig. 2(c). We notice that the height of the conductivity peak is β dependent. For example, for σ_{xx} peak of $n = 0$, the peak height increases gradually as β increases from 0 to 0.8. This is different from the DOS peak which is β independent, as shown in Figs. 2(d) and 2(e). In addition, the conductivity peak is anisotropic. For example, $\sigma_{xx}(0)$ increases gradually as β increases from 0 to 0.8, while $\sigma_{yy}(0)$ in Fig. 6(b) decreases gradually as β increases from 0 to 0.8. To see the quantitative dependence of the heights of σ_{xx} and σ_{yy} peaks on β, we plot their peak values of $n = 0$, 1, and 2 as functions of β in Fig. 6(c). It is obvious that with the increase of β, $\sigma_{xx}(0)$ increases but $\sigma_{yy}(0)$ diminishes. σ_{xx} peaks of $n = 1$ and 2 are less dependent on β in the range of $\beta \leqslant 0.6$. In contrast, the correspond σ_{yy} peaks decrease nontrivially with β. According to the data in Fig. 6(c), we get $\sigma_{xx}(0)/\sigma_{yy}(0) \simeq 1/(1-\beta^2)$, while $\sigma_{xx}(\varepsilon_n)/\sigma_{yy}(\varepsilon_n) < 1/(1-\beta^2)$ for $n = 1$ and 2, which are shown in Fig. 6(d). Such a

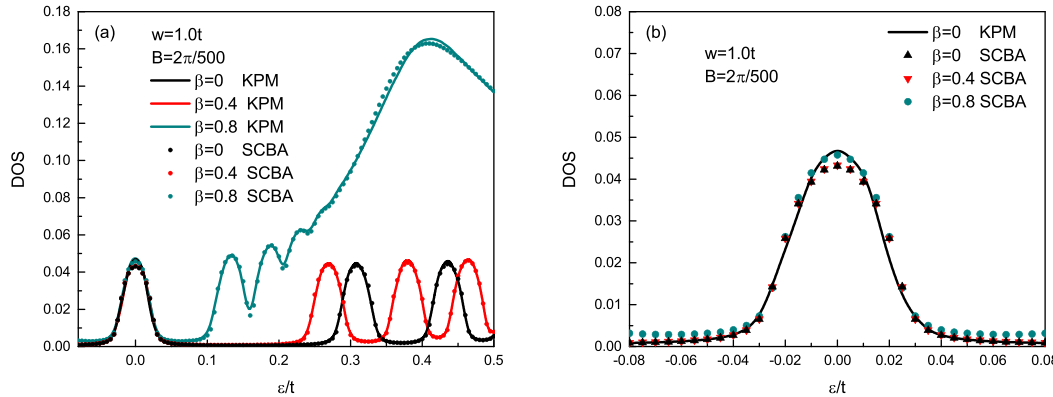

FIG. 5. (a) A comparison of the DOS of the systems with typical cone tilt computed by using KPM and SCBA. (b) Enlarged views of the zero energy peaks in (a).

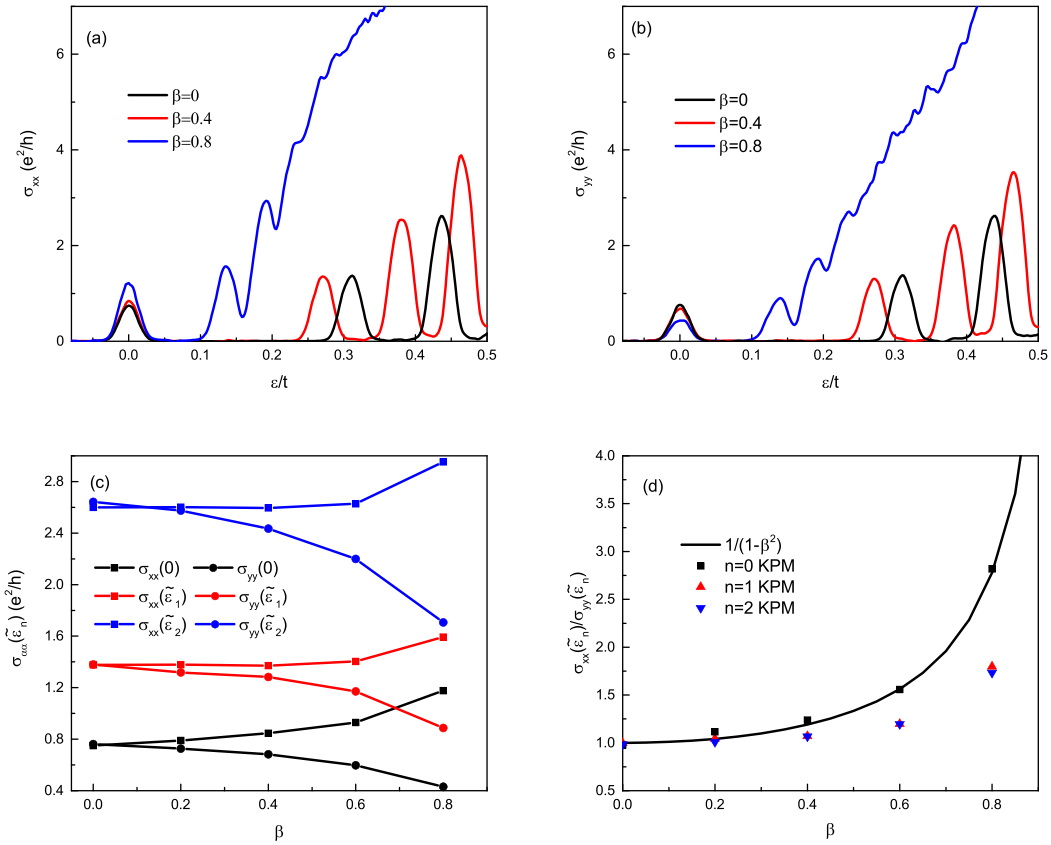

FIG. 6. The DC spectra $\sigma_{xx}(\varepsilon)$ (a) and $\sigma_{yy}(\varepsilon)$ (b) of the three systems with $\beta = 0$, 0.4, and 0.8. (c) The DC peaks $\sigma_{xx}(\widetilde{\varepsilon}_n)$ and $\sigma_{yy}(\widetilde{\varepsilon}_n)$ of $n = 0$, 1 and 2 as functions of β. It should be noted that $\widetilde{\varepsilon}_n$ is the energy position of the redshifted LL peak, not the LL ε_n of the clean system. (d) the ratio $\sigma_{xx}(\widetilde{\varepsilon}_n)/\sigma_{yy}(\widetilde{\varepsilon}_n)$ of $n = 0$, 1, and 2 as functions of β. Here, the disorder strength and magnetic field are fixed at $w = 1.0t$ and $B = 2\pi/500$, respectively.

result is the same as that of a clean system, which means that the anisotropy of diagonal conductivity caused by the cone tilt is retained in the presence of disorder, at least for the disorder with the strength smaller than $w = 1.0t$.

Next, we examine the effect of the disorder strength on diagonal conductivity. We choose the system with $\beta = 0$ to calculate $\sigma_{xx}(\varepsilon)$ with different w. The magnetic-field strength is still fixed at $B = 2\pi/500$. Figure 7(a) shows $\sigma_{xx}(\varepsilon)$ in the cases of $w = 1.0t$ and $2.0t$. Here, the results from SCBA are also shown for comparison. First, let us look at the results from KPM, which are shown by the red and blue solid lines in Fig. 7(a). It can be seen that the stronger the disorder, the wider the σ_{xx} peaks and the larger the redshifts of the σ_{xx} peaks, which are similar to the behavior of the LL peaks in

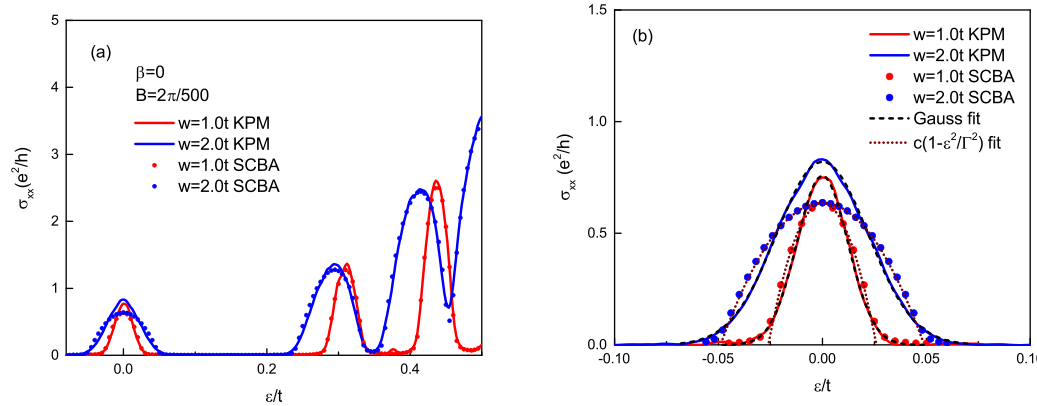

FIG. 7. (a) The DC spectra $\sigma_{xx}(\varepsilon)$ of the system with $\beta = 0$ in the cases of $w = 0.1t$ and $2.0t$. The results from SCBA are also shown for comparison. (b) Enlarged views of the zero energy σ_{xx} peaks in (a). Here, the σ_{xx} peaks form KPM are fitted well by a Gaussian function $C\exp(-\varepsilon^2/2\Gamma^2)/\Gamma$, while the σ_{xx} peaks form SCBA are fitted well by the function $C(1-\varepsilon^2/\Gamma^2)$.

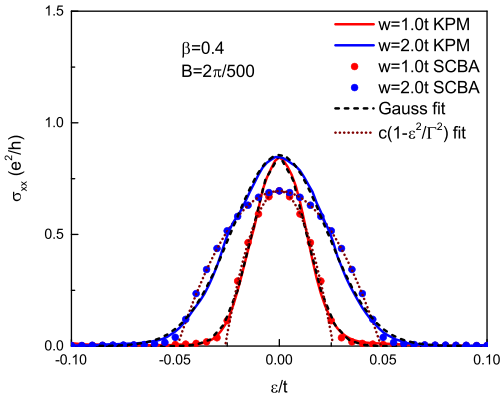

FIG. 8. The zero energy σ_{xx} peaks of the system with $\beta = 0.4$ computed by using KPM and SCBA. Here, the σ_{xx} peaks form KPM are still fitted well by a Gaussian function $c\exp(-\varepsilon^2/2\Gamma^2)/\Gamma$, and the σ_{xx} peaks form SCBA are still fitted well by the function $c(1 - \varepsilon^2/\Gamma^2)$.

the DOS spectrum shown in Fig. 2(a). However, unlike the LL peaks in DOS whose heights decrease with the increase of w, the heights of the σ_{xx} peaks do not change significantly with the increase of w from $1.0t$ to $2.0t$. Moreover, it is seen that $\sigma_{xx}(0)$ with $w = 2.0t$ is slightly higher than that with $w = 1.0t$. We verify that the σ_{xx} peaks around zero energy are a Gaussian type, the same type as the DOS peaks, as shown by the black dashed line in Fig. 7(b). Now let us compare the results from SCBA and KPM. As one can see in Fig. 7(a), the two sets of data are in agreement in terms of the broadenings and redshifts of the σ_{xx} peaks in both cases of $w = 1.0t$ and $2.0t$. The remarkable difference between the two sets of data occurs near zero energy, similar to that in the DOS spectrum. However, the difference in the σ_{xx} spectrum is more significant, which can be seen in Fig. 7(b). One may notice that the heights of the σ_{xx} peaks from SCBA are w independent and $\sigma_{xx}(0) = 0.636e^2/h$, which is equal to the zero-energy conductivity of graphene reported by SCBA [24]. In view of this, SCBA is not competent to describe the dependence of zero-energy conductivity on disorder. One may also notice that the σ_{xx} peaks under SCBA are neither a Gaussian type nor a semielliptical type like the DOS peaks, but are well fitted by a function $C(1 - \varepsilon^2/\Gamma^2)$ with C and Γ being fitting parameters. Therefore, just like the case in the DOS spectrum, SCBA also fails to describe the shape of the zero-energy conductivity peak.

Furthermore, we numerically simulate the $\sigma_{xx}(\varepsilon)$ of the system with $\beta = 0.4$ in the cases of $w = 1.0t$ and $2.0t$ by KPM and SCBA. The $\sigma_{xx}(\varepsilon)$ around zero energy are shown in Fig. 8. They are similar to those in Fig. 7(b). The $\sigma_{xx}(\varepsilon)$ from SCBA deviate significantly from those from KPM at zero energy. In the presence of the tilt of Dirac cone, the σ_{xx} peaks from SCBA can still be fitted by the function $C(1 - \varepsilon^2/\Gamma^2)$, and the σ_{xx} peaks from KPM are still well fitted by Gaussian function. Compared with the SCBA results of the system with $\beta = 0$ in Fig. 7(b), the SCBA results of the system with $\beta = 0.4$ show that $\sigma_{xx}(0) = 0.695e^2/h$ is larger. Therefore, the SCBA results also show that the tilt of the Dirac cone leads to the increase of the σ_{xx} peak. In addition, different from the KPM results of the system with $\beta = 0$, whose $\sigma_{xx}(0)$ is w dependent and increases with w, the KPM results of the system with $\beta = 0.4$ show that the $\sigma_{xx}(0)$ takes almost the same value in both cases of $w = 1.0$ and $2.0t$. This implies that the $\sigma_{xx}(0)$ for the system with $\beta = 0.4$ is saturated when disorder strength reaches $1.0t$, while the $\sigma_{xx}(0)$ for the system with $\beta = 0$ has not reached saturation at $w = 1.0t$. In other words, the tilt of Dirac cone makes the zero energy conductivity reach saturation under relatively weak disorder strength.

Above, we have calculated the diagonal conductivities as functions of Fermi energy with a fixed magnetic field strength B to show the tilt effect of Dirac cone in the conductivity spectrum. It is convenient for theoretical study. However, in magnetotransport measurements, tuning the Fermi energy is not easy. Instead, the magnetic field is controllable when the number of the carrier is fixed. Therefore, the spectrum of the conductivity $\sigma_{\alpha\alpha}$ versus $1/B$ is usually provided in experiments. We would like to say that the two alternatives, $\sigma_{\alpha\alpha}$ versus Fermi energy in theory and $\sigma_{\alpha\alpha}$ versus $1/B$ from experimental measure, can well uncover the basic features of quantum magnetotransport in the 2D system, namely, when the quantized LLs pass through the Fermi surface in a one-by-one way, the conductivity exhibits discrete peaks (in the quantum Hall regime) or Shubnikov-de Haas (SdH) oscillation. However, the profile details of the two kinds of conductivity spectra can be different, for example, the conductivity peaks in $\sigma_{\alpha\alpha}(\varepsilon_F)$ are not equidistant, which reflects the LL spectrum, while the conductivity peaks in $\sigma_{\alpha\alpha}(1/B)$ are equidistant. In experiments, with the increase of $1/B$ (the magnetic field gets weaker), the system transforms from quantum Hall to SdH oscillation regime. In the SdH oscillation regime, the overlap between the adjacent LL peaks occurs due to the disorder broadening. It is obvious that the cone tilt makes the SdH oscillation to occur early, i.e., in a relatively strong magnetic field range. This is because the cone tilt can squeeze the LL spectrum efficiently. As a result, the overlap between the adjacent LL peaks occurs even in a relatively weak disorder, in contrast with the case without cone tilt. However, the cone tilt does not affect the oscillation period, which is determined by the area of the Fermi surface. For a fixed number of carriers, the Fermi energy of the tilted system is lower than that of the nontilted system but the areas of the Fermi surfaces of the two systems are still the same and so the oscillation periods are the same. Besides, it is a reasonable prediction that the conductivity anisotropy arising from the cone tilt as discussed above can be observed in the SdH regime of the experimental $\sigma_{\alpha\alpha}$ versus $1/B$ spectrum.

IV. CONCLUSIONS

In summary, we investigate the effects of Dirac cone tilt on the disorder-broadened LLs in a 2D Dirac system. For this purpose, based on a lattice model of a 2D Dirac system that hosts two Dirac cones with adjustable tilt and with random on-site disorder, and by means of KPM which is a numerically exact theoretical approach, we calculate the DOS and diagonal conductivity as a function of Fermi energy in the presence of a high magnetic field. Our numerical results show that the tilt of the Dirac cone squeezes the LL spectrum and makes the LL peaks become denser, which drives the system to

leave the quantum Hall regime under relatively weak disorder. However, in the quantum Hall regime, the broadening of an isolated LL peak in the DOS spectrum is tilt independent. As a result, the features of the isolated LL peak are the same as those of graphene. The diagonal conductivity is tilt dependent and anisotropic. The Dirac cone tilt enhances the diagonal conductivity peaks in the direction perpendicular to the tilt but reduces the diagonal conductivity peaks in the direction parallel to the tilt. For the zero-energy LL, the ratio of the former to the latter is $\sigma_{xx}(0)/\sigma_{yy}(0) = 1/(1-\beta^2)$, with β being the tilt parameter. This means that the anisotropy of diagonal conductivity increases with β. In contrast, for the nonzero LL peaks, such a ratio is relatively small, $\sigma_{xx}(\varepsilon_n)/\sigma_{yy}(\varepsilon_n) < 1/(1-\beta^2)$.

In addition, in comparison with the results obtained by KPM, we check the validity of SCBA which has thus far been widely exploited for studying the DOS and quantum transport properties of Dirac and Weyl systems with disorder. Our numerical results indicate that though at first sight the global DOS and diagonal conductivity spectra composed of multiple LL peaks given by SCBA agree with those obtained by KPM as far as the broadenings and redshifts of the disorder-broadened LL peaks are concerned, but SCBA fails to describe the details of the LL peaks around zero energy in both the DOS and diagonal conductivity spectra. The results obtained by KPM show that the zero-energy LL peaks in both the DOS and diagonal conductivity spectra are Gaussian types, while the results under SCBA show that the LL peak in the DOS spectrum is a semiellipse type and the LL peak in the conductivity spectrum is neither a Gaussian type nor a semiellipse type, but is well fitted by a function $C(1-\varepsilon^2/\Gamma^2)$. What is more, at zero energy, the KPM result of the diagonal conductivity increases with the disorder strength before saturation rather than a disorder-independent constant as reported previously by SCBA.

Before ending this paper, we would like to make a comparison of the Landau quantization between the 3D and 2D Dirac nodal systems, focusing on the cone tilt effect. The LL spectra of clean 3D Weyl or Dirac nodal systems with type-I and type-II cone tilts were reported in previous literature [34,35,40,41]. In the presence of a magnetic field, the electronic eigenenergy spectra of these 3D systems reduce to 1D Landau subbands with the residual dispersion paralleling to the magnetic-field direction (set as z direction), and by fixing $k_z = 0$ these 1D Landau subbands just reduce to the discrete LLs of 2D Dirac nodal systems with the same tilt. Due to such a 1D Landau subband structure, the DOS and diagonal conductivity spectra of 3D Weyl or Dirac nodal systems have different aspects in the profile from the case of 2D Dirac nodal system studied in this paper [27]. First, both the DOS peak and conductivity peak around zero energy are missing due to the chirality of the $n = 0$ Landau subband. Besides, the shapes of other DOS and conductivity peaks are also different from their counterparts in 2D system. Despite these profile differences, the DOS and conductivity peaks in either the 2D or 3D system suffer from the same squeezing effects by the cone tilt perpendicular to the magnetic field [35]. In addition, the unique eight-shaped cyclotron resonance orbital and the magnetic breakdown between the electron and hole pockets caused by type-II tilt are also the common phenomena for 3D and 2D systems. According to the theoretical results for 3D systems [31,42,43], it can be found that with the increase of cone tilt, the peak heights of the conductivity perpendicular to the tilt direction increase, whereas the peak heights of the conductivity parallel to the tilt direction decrease. Such an effect is similar to that in the 2D system discussed above. However, it should be pointed out that the theoretical results of the 3D system reported previously were limited to the case that the magnetic field is parallel to the tilt direction, while the 2D system we consider is subject to an out-of-plane magnetic field. Thus, the magnetic field is perpendicular to the tilt direction, so both σ_{xx} and σ_{yy} refer to the transverse conductivity (relative to the magnetic-field direction). As far as we know, the anisotropy of two transverse conductivities in a 3D system with a magnetic field perpendicular to the tilt direction has not been reported in literature.

ACKNOWLEDGMENTS

This work was financially supported by the National Natural Science Foundation of China (Grant No. 11774123) and the Natural Science Foundation of Jilin Province of China (Grant No. 20190201123JC). We thank the High Performance Computing Center of Jilin University for their computational resources.

APPENDIX A: THE LLs OF $H_{0\eta}(\boldsymbol{k})$ IN THE PRESENCE OF A MAGNETIC FIELD

We take $H_{0-}(\boldsymbol{k})$ as the representative to show the eigensolution of LLs of a Dirac cone with tilt. The effective Hamiltonian reads

$$H_{0-}(\boldsymbol{k}) = \gamma(k_x\sigma_x + k_y\sigma_y + \beta k_y\sigma_0). \tag{A1}$$

In the presence of a magnetic field $\boldsymbol{B} = (0, 0, B)$, we make the usual Peierls substitution $\boldsymbol{k} \to \boldsymbol{k} + e\boldsymbol{A}/\hbar$ and choose the Landau gauge $\boldsymbol{A} = (0, Bx, 0)$. Then, only k_y remains as a good quantum number, the above Hamiltonian turns to

$$H_B = \gamma\left[\widehat{k}_x\sigma_x + \left(k_y + l_B^{-2}x\right)\sigma_y + \beta l_B^{-2}x\sigma_0 + \beta k_y\sigma_0\right], \tag{A2}$$

with $\widehat{k}_x = -i\partial_x$ and $l_B = \sqrt{\hbar/eB}$ being the magnetic length, which is reminiscent of an effective 2D Dirac system with a translation term in energy $\gamma\beta k_y$ under a magnetic field $\boldsymbol{B} = (0, 0, B)$ and an effective electric field $E_{\text{eff}} = \gamma\beta l_B^{-2}\widehat{e}_x$. When $\beta < 1$, the effective electric field can be eliminated by a Lorentz boost [33]. By means of the Lorentz boost method, we obtain the exact eigensolution of H_B. The LLs are

$$\varepsilon_n = \text{sgn}(n)\sqrt{2|n|}\gamma l_B^{-1}(1-\beta^2)^{3/4} \tag{A3}$$

where $n = 0, \pm1, \pm2...$ is Landau index. The corresponding eigenfunctions are given by

$$\Psi_{nk_y}(\boldsymbol{r}) = \frac{C_n}{\sqrt{L}}\exp(ik_y y)\exp(-\sigma_y\theta/2)\begin{pmatrix}\text{sgn}(n)\varphi_{|n|-1}(\xi)\\ i\varphi_{|n|}(\xi)\end{pmatrix}, \tag{A4}$$

with

$$C_n = \begin{cases}\frac{1}{\sqrt{\cosh^2(\theta/2)+\sinh^2(\theta/2)}} & (n=0)\\ \frac{1}{\sqrt{2[\cosh^2(\theta/2)+\sinh^2(\theta/2)]}} & (n\neq 0),\end{cases} \tag{A5}$$

$$\exp(-\sigma_y\theta/2) = \cosh(\theta/2) - \sigma_y\sinh(\theta/2), \tag{A6}$$

and

$$\mathrm{sgn}(n)=\begin{cases}1 & (n>0)\\ 0 & (n=0)\\ -1 & (n<0),\end{cases} \tag{A7}$$

where $\tanh(\theta)=\beta$, so $\cosh^2(\theta/2)+\sinh^2(\theta/2)=1/\sqrt{1-\beta^2}$, $\varphi_{|n|-1}(\xi)$ and $\varphi_{|n|}(\xi)$ are the harmonic oscillator eigenfunctions but the scaled x coordinate $\xi=(1-\beta^2)^{1/4}(x+l_B^2k_y)l_B^{-1}+\mathrm{sgn}(n)\sqrt{2|n|}\beta$ is dependent on Landau index n. From Eqs.(A4)–(A7), we find that compared with the case without tilt, that is, $\beta=0$, the tilt of the Dirac cone brings about three properties: an introduced Hermitian matrix $\exp(-\sigma_y\theta/2)$, β-dependent normalization coefficient C_n, and n-dependent local center of $\varphi_{|n|-1}(\xi)$ and $\varphi_{|n|}(\xi)$ in Eq. (A4).

To understand the anisotropy of the diagonal conductivity caused by Dirac cone tilt, we next calculate the matrix elements of the velocity operators v_x and v_y in the eigenrepresentation. According to $\boldsymbol{v}=[\boldsymbol{r},H_B]/i\hbar$, we can get $v_x=\gamma\sigma_x/\hbar$ and $v_y=\gamma(\sigma_y+\beta\sigma_0)/\hbar$. Let $|nk_y\rangle$ represent the eigenstate of H_B, i.e., $\langle\boldsymbol{r}|nk_y\rangle=\Psi_{nk_y}(\boldsymbol{r})$, it is easy to check that $\langle nk_y|v_{x/y}|n'k'_y\rangle=\langle nk_y|v_{x/y}|n'k_y\rangle\delta_{k_y,k'_y}(1-\delta_{n,n'})$, that is, the diagonal elements of the velocity operator are all zero. Other off diagonal elements are calculated as follows:

$$\langle nk_y|v_x|n'k_y\rangle=\frac{i\gamma}{\hbar}C_nC_{n'}[\mathrm{sgn}(n)W_{|n|-1,|n'|}-\mathrm{sgn}(n')W_{|n|,|n'|-1}] \tag{A8}$$

and

$$\langle nk_y|v_y|n'k_y\rangle=\frac{\gamma\sqrt{1-\beta^2}}{\hbar}C_nC_{n'}[\mathrm{sgn}(n)W_{|n|-1,|n'|}+\mathrm{sgn}(n')W_{|n|,|n'|-1}], \tag{A9}$$

with $W_{k,l}=\int\varphi_k(\xi)\varphi_l(\xi')d\boldsymbol{x}$. It is worth noting that in this integral, the variables ξ and ξ' of $\varphi_k(\xi)$ and $\varphi_l(\xi')$ are different, they depend on Landau index n and n', respectively. Thus, $W_{k,l}$ does not represent the orthogonal or normalization formula of the harmonic oscillator eigenfunction. In other words, one has $W_{k,l}\neq 0$ if $k\neq l$ and $W_{k,l}\neq 1$ if $k=l$. Therefore, in Eqs. (A8) and (A9), both $W_{|n|-1,|n'|}$ and $W_{|n|,|n'|-1}$ are nonzero, which is different from the case without tilt, in which at most one of the two terms is nonzero. We check that both $W_{|n|-1,|n'|}$ and $W_{|n|,|n'|-1}$ are always greater than zero for any n and n'. So it is easy to find that when $n=0$ or $n'=0$, $|\langle nk_y|v_x|n'k_y\rangle|^2/|\langle nk_y|v_y|n'k_y\rangle|^2=1/(1-\beta^2)$, while when $n,n'\neq 0$ and $\mathrm{sgn}(nn')>0$, $|\langle nk_y|v_x|n'k_y\rangle|^2/|\langle nk_y|v_y|n'k_y\rangle|^2<1/(1-\beta^2)$. Such a result indicates that the tilt of Dirac cone results in a tilt-dependent and anisotropic diagonal conductivity, as discussed in Sec. II.

APPENDIX B: KPM

KPM works by expanding the delta operator in Eqs. (5) and (6) in terms of the Chebyshev polynomials of the first kind, $T_n(x)=\cos[n\arccos(x)]$. For this purpose, the Hamiltonian needs to be rescaled so the corresponding energy spectrum is dimensionless and stays in the range of $[-1,1]$. For a lattice Hamiltonian, the eigenenergy is distributed in the range of $[\varepsilon_{\min},\varepsilon_{\max}]$. We rescale the Hamiltonian and the Fermi energy as $\widetilde{H}=(H-B)/W$ and $\widetilde{\varepsilon}=(\varepsilon-B)/W$, where $W=(\varepsilon_{\max}-\varepsilon_{\min})/2$ and $B=(\varepsilon_{\max}+\varepsilon_{\min})/2$. Then, the rescaled delta operator in Eqs. (5) and (6) can be expanded in terms of the Chebyshev polynomials as

$$\delta(\widetilde{\varepsilon}-\widetilde{H})\simeq\frac{2}{\pi\sqrt{1-\widetilde{\varepsilon}^2}}\sum_{n=0}^{M-1}g_n\frac{T_n(\widetilde{\varepsilon})}{\delta_{n,0}+1}T_n(\widetilde{H}). \tag{B1}$$

In Eq. (B1), the approximately equal sign appears because the Chebyshev polynomials is truncated at a finite M-term series. This truncation often leads to Gibbs oscillation. For this reason, a kernel g_n is introduced to smear out the oscillation. Among several alternative kernels, we choose the Lorentz kernel in this paper, i.e., $g_n=\sinh[\lambda(1-n/M)]/\sinh\lambda$, where λ is an empirical parameter in the range of $3\sim 5$. In addition, this truncation also introduces an artificial width to the expanded delta function, which is determined by $\eta\simeq\lambda/M$. In our calculation, we set $\lambda=3$ and $M=6000$, so the artificial width η is about $4\times10^{-3}t$ after considering the rescaling of energy.

Substituting Eq. (B1) into Eqs. (5) and (6), we obtain

$$\rho(\widetilde{\varepsilon})\simeq\frac{2}{\pi NW\sqrt{1-\widetilde{\varepsilon}^2}}\sum_{n=0}^{M-1}\frac{g_n}{\delta_{n,0}+1}\mu_nT_n(\widetilde{\varepsilon}), \tag{B2}$$

$$\sigma_{\alpha\alpha}(\widetilde{\varepsilon})\simeq\frac{4e^2\hbar}{\pi S}\frac{1}{1-\widetilde{\varepsilon}^2}\sum_{n,m=0}^{M-1}\frac{g_ng_m}{(\delta_{n,0}+1)(\delta_{m,0}+1)}\times\mu_{nm}^{\alpha\alpha}T_n(\widetilde{\varepsilon})T_m(\widetilde{\varepsilon}), \tag{B3}$$

where $\mu_n=\mathrm{Tr}[T_n(\widetilde{H})]$ and $\mu_{nm}^{\alpha\alpha}=\mathrm{Tr}[\widetilde{v}_\alpha T_n(\widetilde{H})\widetilde{v}_\alpha T_m(\widetilde{H})]$. The first two Chebyshev polynomials are $T_0(\widetilde{H})=1$ and $T_1(\widetilde{H})=\widetilde{H}$, and for $n\geqslant 2$, we have the recursive relation: $T_n(\widetilde{H})=2\widetilde{H}T_{n-1}(\widetilde{H})-T_{n-2}(\widetilde{H})$. The computations of μ_n and $\mu_{nm}^{\alpha\alpha}$ are the most time-consuming parts in Eqs. (B2) and (B3), respectively.

For a disordered system, using a random phase state can significantly improve the efficiency of evaluating the traces such as μ_n and $\mu_{nm}^{\alpha\alpha}$. The random phase state is defined as $|\psi_j\rangle=\sum_{k=1}^{N}e^{2\pi i\gamma_k^j}|r_k\rangle/\sqrt{N}$ with γ_k^j being a set of random numbers uniformly distributed in the region of [0,1] and $|r_k\rangle$ being the base vector in the tight-binding model [38,39]. For a given disordered sample, we use N_R random phase states to evaluate the traces $\mathrm{Tr}[\cdots]=N\sum_{j=1}^{N_R}\langle\psi_j|\cdots|\psi_j\rangle/N_R$. And then we also need to average over N_s different disorder samples. Because of the self-average property of the random phase states, $N_R\times N_s$ could be much less than the dimension of the system N. In our simulation, $N=5\times10^5$, however, we only actually calculate $N_R\times N_s$ different matrix elements to simulate these two traces for the system with a given w. For the calculation of DOS, the results are well convergent when $N_R\times N_s>150$ in all cases considered in this paper. For the calculation of the diagonal conductivity, a slightly larger $N_R\times N_s$ is required to bring about a convergent result, especially in the case of large w. For example, convergence is reached when $N_R\times N_s>300$ in the case of $w=1.0t$, whereas convergence requires $N_R\times N_s>700$ in the case of $w=2.0t$.

APPENDIX C: SCBA

Within the framework of SCBA, we need to introduce the disorder-averaged Green's function to express the delta

operator function in Eqs. (5) and (6). The Green's function is defined as

$$\overline{G}^R(\varepsilon) = \left\langle \frac{1}{\varepsilon - H_0 - H_d + i\eta} \right\rangle = \frac{1}{\varepsilon - H_0 - \Sigma(\varepsilon) + i\eta}, \tag{C1}$$

where $\langle\rangle$ means the average over the disorder configurations, $\Sigma(\varepsilon)$ is the average self-energy, and η is an artificial infinitesimal. To compare with the results from KPM, we set the η to be the same as that in KPM. Under SCBA, the average self-energy is calculated by the self-consistency equation

$$\begin{aligned}\Sigma(\varepsilon) &= \frac{\int_{-\frac{w}{2}}^{\frac{w}{2}} \epsilon^2 d\epsilon}{w} \langle r_i s|\overline{G}^R(\varepsilon)|r_i s\rangle \\ &= \frac{w^2}{12}\int_{\mathrm{MBZ}} \frac{d\boldsymbol{k}}{(2\pi)^2/N_y} \langle n_i s|\bar{G}^R_{\boldsymbol{k}}(\varepsilon)|n_i s\rangle \end{aligned} \tag{C2}$$

where $|r_i s\rangle$ denotes a lattice state at any site r_i and orbital s on the square lattice, $|n_i s\rangle$ denotes a lattice state in the magnetic suppercell, $\bar{G}^R_{\boldsymbol{k}}(\varepsilon) = [\varepsilon - H_{\boldsymbol{k}} - \Sigma(\varepsilon) + i\eta]^{-1}$ with $H_{\boldsymbol{k}}$ is the Hamiltonian of the clean system with the magnetic supercell as the primitive cell, and the integration being performed over the magnetic Brillouin zone (MBZ). Although the translational symmetry is broken by the magnetic field in real space, it is restored by the Peierls substitution within the magnetic supercell. Thus, in Eq. (C2), the dimension of the Green's function can be reduced from the dimension of the system to the dimension of the magnetic supercell. With the retard Green's function $\bar{G}^R_{\boldsymbol{k}}(\varepsilon)$ and the corresponding advanced Green's function $\bar{G}^A_{\boldsymbol{k}}(\varepsilon) = [\bar{G}^R_{\boldsymbol{k}}(\varepsilon)]^\dagger$, the DOS and diagonal conductivity can be expressed as

$$\rho(\varepsilon) = -\int_{\mathrm{MBZ}} \frac{d\boldsymbol{k}}{(2\pi)^3} \mathrm{Tr}\big[\mathrm{Im}\big(G^R_{\boldsymbol{k}} - G^A_{\boldsymbol{k}}\big)\big], \tag{C3}$$

$$\sigma_{\alpha\alpha}(\varepsilon) = \frac{e^2\hbar}{4\pi S}\sum_{\boldsymbol{k}} \mathrm{Tr}\big[v_\alpha \mathrm{Im}\big(G^R_{\boldsymbol{k}} - G^A_{\boldsymbol{k}}\big) v_\alpha \mathrm{Im}\big(G^R_{\boldsymbol{k}} - G^A_{\boldsymbol{k}}\big)\big]. \tag{C4}$$

[1] A. H. Castro Neto, F. Guinea, N. M. R. Peres, K. S. Novoselov, and A. K. Geim, Rev. Mod. Phys. **81**, 109 (2009).
[2] S. Das Sarma, S. Adam, E. H. Hwang, and E. Rossi, Rev. Mod. Phys. **83**, 407 (2011).
[3] K. S. Novoselov, A. K. Geim, S. V. Morozov, D. Jiang, M. I. Katsnelson, I. V. Grigorieva, S. V. Dubonos, and A. A. Firsov, Nature (London) **438**, 197 (2005).
[4] W. Zhu, Q. W. Shi, X. R. Wang, J. Chen, J. L. Yang, and J. G. Hou, Phys. Rev. Lett. **102**, 056803 (2009).
[5] W. Zhu, H. Y. Yuan, Q. W. Shi, J. G. Hou, and X. R. Wang, Phys. Rev. B **83**, 153408 (2011).
[6] F. Wegner, Z. Phys. B **51**, 279 (1983).
[7] F. Ortmann and S. Roche, Phys. Rev. Lett. **110**, 086602 (2013).
[8] S. M. Choi, S. H. Jhi, and Y. W. Son, Phys. Rev. B **81**, 081407(R) (2010).
[9] H. Y. Lu, A. S. Cuamba, S. Y. Lin, L. Hao, R. Wang, H. Li, Y. Y. Zhao, and C. S. Ting, Phys. Rev. B **94**, 195423 (2016).
[10] M. O. Goerbig, J. N. Fuchs, G. Montambaux, and F. Piechon, Phys. Rev. B **78**, 045415 (2008).
[11] A. Mori, M. Sato, T. Yajima, T. Konoike, K. Uchida, and T. Osada, Phys. Rev. B **99**, 035106 (2019).
[12] A. Kobayashi, S. Katayama, Y. Suzumura, and H. Fukuyama, J. Phy. Soc. Jpn. **76**, 034711 (2007).
[13] M. Hirata, K. Ishikawa, K. Miyagawa, M. Tamura, C. Berthier, D. Basko, A. Kobayashi, G. Matsuno, and K. Kanoda, Nat. Commun. **7**, 12666 (2016).
[14] X. F. Zhou, X. Dong, A. R. Oganov, Q. Zhu, Y. J. Tian, and H. T. Wang, Phys. Rev. Lett. **112**, 085502 (2014).
[15] A. D. Zabolotskiy and Y. E. Lozovik, Phys. Rev. B **94**, 165403 (2016).
[16] B. Feng, O. Sugino, R.Y. Liu, J. Zhang, R. Yukawa, M. Kawamura, T. Iimori, H. Kim, Y. Hasegawa, H. Li, L. Chen, K. Wu, H. Kumigashira, F. Komori, T.C. Chiang, S. Meng, I. Matsuda, and I. Matsuda, Phys. Rev. Lett. **118**, 096401 (2017).
[17] SK Firoz Islam and A. M. Jayannavar, Phys. Rev. B **96**, 235405 (2017).
[18] Y. Tanaka, Z. Ren, T. Sato, K. Nakayama, S. Souma, T. Takahashi, K. Segawa, and Y. Ando, Nat. Phys. **8**, 800 (2012).
[19] I. Sodemann and L. Fu, Phys. Rev. Lett. **115**, 216806 (2015).
[20] S. H. Zhang and W. Yang, Phys. Rev. B **97**, 235440 (2018).
[21] V. H. Nguyen and J. C. Charlier, Phys. Rev. B **97**, 235113 (2018).
[22] K. Sadhukhan and A. Agarwal, Phys. Rev. B **96**, 035410 (2017).
[23] S. Verma, A. Mawrie, and T. K. Ghosh, Phys. Rev. B **96**, 155418 (2017).
[24] Y. S. Zheng and T. Ando, Phys. Rev. B **65**, 245420 (2002).
[25] M. Koshino and T. Ando, Phys. Rev. B **73**, 245403 (2006).
[26] Y. Ominato and M. Koshino, Phys. Rev. B **89**, 054202 (2014).
[27] J. Klier, I. V. Gornyi, and A. D. Mirlin, Phys. Rev. B **92**, 205113 (2015).
[28] Y. Ominato and M. Koshino, Phys. Rev. B **91**, 035202 (2015).
[29] M. Trescher, B. Sbierski, P. W. Brouwer, and E. J. Bergholtz, Phys. Rev. B **95**, 045139 (2017).
[30] J. Klier, I. V. Gornyi, and A. D. Mirlin, Phys. Rev. B **100**, 125160 (2019).
[31] Y. X. Wang and F. X. Li, Phys. Rev. B **101**, 085201 (2020).
[32] I. L. Aleiner and K. B. Efetov, Phys. Rev. Lett. **97**, 236801 (2006).
[33] V. Lukose, R. Shankar, and G. Baskaran, Phys. Rev. Lett. **98**, 116802 (2007).
[34] M. Koshino, Phys. Rev. B **94**, 035202 (2016).
[35] Z.-M. Yu, Y. Yao, and S. A. Yang, Phys. Rev. Lett. **117**, 077202 (2016).
[36] M. J. Park, B. Basa, and M. J. Gilbert, Phys. Rev. B **95**, 094201 (2017).
[37] C. Z. Chen, J. Song, H. Jiang, Q. F. Sun, Z. Wang, and X. C. Xie, Phys. Rev. Lett. **115**, 246603 (2015).

[38] Z. Liu, M. F. Zhu, and Y. S. Zheng, Phys. Rev. B **92**, 245438 (2015).
[39] A. Weisse, G. Wellein, A. Alvermann, and H. Fehske, Rev. Mod. Phys. **78**, 275 (2006).
[40] S. Tchoumakov, M. Civelli, and M. O. Goerbig, Phys. Rev. Lett. **117**, 086402 (2016).
[41] T. E. O'Brien, M. Diez, and C. W. J. Beenakker, Phys. Rev. Lett. **116**, 236401 (2016).
[42] A. Ahmad and G. Sharma, Phys. Rev. B **103**, 115146 (2021).
[43] L. Feng, T. Ma, and Y. Zheng, J. Phys.: Condens. Matter **32**, 205502 (2020).